



CrossMark
 click for updates

Cite this: *RSC Adv.*, 2017, 7, 2615

Efficient green electroluminescence based on an iridium(III) complex with different device structures†

Yi-Ming Jing,^a You-Xuan Zheng^{*abc} and Jing-Lin Zuo^a

A series of phosphorescent organic light-emitting diodes (OLEDs) with single or double light-emitting layer(s) were fabricated using a green iridium(III) complex Ir(BTBP)₂POP containing 2',6'-bis(trifluoromethyl)-2,4'-bipyridine (BTBP) cyclometalated ligand and 2-(5-phenyl-1,3,4-oxadiazol-2-yl) phenol (POP) ancillary ligand. The single light-emitting layer devices with the structure of ITO/MoO₃ (5 nm)/TAPC (1,1-bis[4-(di-*p*-tolylamino)phenyl]cyclohexane, 30 nm)/mCP (*N,N'*-dicarbazolyl-3,5-benzene, 5 nm)/Ir(BTBP)₂POP:PPO21 (3-(diphenylphosphoryl)-9-(4-(diphenylphosphoryl)phenyl)-9*H*-carbazole, 8 wt%, 10 nm)/TmPyPB (1,3,5-tri(*m*-pyrid-3-yl-phenyl)benzene, 40 nm)/LiF (1 nm)/Al (100 nm) achieved the highest luminance, current efficiency, power efficiency and external quantum efficiency (EQE) up to 47 599 cd m⁻², 86.5 cd A⁻¹, 52.2 lm W⁻¹ and 31.0%, respectively. Furthermore, the double EML device with the structure of ITO/MoO₃ (5 nm)/TAPC (30 nm)/mCP:Ir(BTBP)₂POP (8 wt%, 10 nm)/PPO21:Ir(BTBP)₂POP (8 wt%, 10 nm)/TmPyPB (40 nm)/LiF (1 nm)/Al (100 nm) obtained a higher maximum luminance of 49 139 cd m⁻² and slightly lower maximum current efficiency, power efficiency and EQE of 75.8 cd A⁻¹, 51.7 lm W⁻¹ and 27.2%, respectively, with lower turn-on voltage. This research suggested that not only the doping concentration but also the thickness of the emissive and electron transport layers strongly affect the EL performances.

Received 21st November 2016
 Accepted 14th December 2016

DOI: 10.1039/c6ra27068a

www.rsc.org/advances

Introduction

Organic light-emitting diodes (OLEDs) have attracted great interest during the last few decades owing to their promising features, including flexibility, color tunability and low power consumption.¹ Phosphorescent transition metal complexes have been widely used in OLEDs as the emitter because phosphors can gather both singlet and triplet excitons therefore accomplishing the theoretical 100% internal quantum efficiency.² Among these complexes, iridium(III) complexes have been intensively studied because of their high phosphorescent quantum efficiency, short lifetime of triplet excited states and broad range of emission colors.³ The strong spin-orbit coupling (SOC) introduced by the central heavy atom can promote the triplet to singlet state radiative transition, which results in

extremely high phosphorescence quantum yields at room temperature.

However, the device efficiency roll-off ratios of many OLEDs with high efficiency using Ir(III) complexes as the emitter are serious, which is mainly due to the deterioration of charge-carrier balance and increase in nonradiative quenching processes including triplet-triplet annihilation (TTA), triplet-polaron annihilation (TPA), and electric-field-induced dissociation of excitons at high current density.⁴ In addition, it is well known that the electron mobility of electron transport materials is roughly 2–3 orders of magnitude lower than the hole mobility of most hole transport materials, the efficiency roll-off of devices is dependent on the capability of electron transport. Therefore, that is essential to use bipolar host materials or synthesize Ir(III) complexes with high electron mobility to achieve phosphorescent OLEDs (PhOLEDs) with low efficiency roll-off.

Recently, our group has developed high efficient PhOLEDs using Ir(III) complexes 2',6'-bis(trifluoromethyl)-2,4'-bipyridine (BTBP) as the main ligand.⁵ The electron affinity would be increased by the nitrogen heterocycle, while the electron mobility of the complexes may be improved by a more negative framework of ligand C[^]N such as bipyridine. Moreover, trifluoromethyl unit could enhance the electron mobility and lead to a better balance of charge injection and transfer. The lower vibrational frequency of the C–F bond would reduce the rate of

^aState Key Laboratory of Coordination Chemistry, Collaborative Innovation Center of Advanced Microstructures, School of Chemistry and Chemical Engineering, Nanjing University, Nanjing 210093, P. R. China. E-mail: yxzheng@nju.edu.cn

^bMaAnShan High-Tech Research Institute of Nanjing University, MaAnShan, 238200, P. R. China

^cState Key Laboratory of Luminescence and Applications, Changchun Institute of Optics, Fine Mechanics and Physics, Chinese Academy of Science, Changchun 130033, P. R. China

† Electronic supplementary information (ESI) available: The synthesis, characterization and properties of the complex. See DOI: 10.1039/c6ra27068a



radiationless deactivation. Furthermore, the bulky CF_3 substituents could affect the molecular packing, and the steric protection around the metal would suppress the self-quenching behavior.⁶ In addition, PhOLEDs based on Ir(III) complexes with 1,3,4-oxadiazole derivatives as ancillary ligands also have good performances owing to their high electron mobility, high photoluminescence quantum yield and good thermal/chemical stability.⁷

In this work, a series of single or double light-emitting layers (EMLs) OLEDs were fabricated with a heteroleptic Ir(III) complex (**Ir(BTBP)₂POP**) using 2',6'-bis(trifluoromethyl)-2,4'-bipyridine (**BTBP**) as the main ligand and 2-(5-phenyl-1,3,4-oxadiazol-2-yl)phenol (**HPOP**) as the ancillary ligand. Finally, efficient green OLEDs with maximum brightness, current efficiency, power efficiency and external quantum efficiency (EQE) up to 47 599 cd m^{-2} , 86.5 cd A^{-1} , 52.2 lm W^{-1} and 31.0%, respectively, was realized by optimizing the doping concentration, the thickness of EML and electron transport layer (ETL).

Results and discussion

OLEDs performance

Device structure and energy level diagram of the OLEDs are depicted in Fig. 1. MoO_3 film was deposited upon indium-tin-oxide (ITO) layer as anode modification layer to improve the injection of holes. TAPC (di-[4-(*N,N*-ditolyl-amino)-phenyl]cyclohexane), which possesses high hole mobility ($\mu_h = 1 \times 10^{-2} \text{ cm}^2 \text{ V}^{-1} \text{ s}^{-1}$), was used as hole transport layer (HTL).⁸ TmPyPB (1,3,5-tri(*m*-pyrid-3-yl-phenyl)benzene), which possesses low-lying HOMO level (−6.70 eV) and high electron mobility ($\mu_e = 1 \times 10^{-3} \text{ cm}^2 \text{ V}^{-1} \text{ s}^{-1}$), was used as hole block/electron transport layer (HBL/ETL).⁹ Bipolar PPO21 (3-(diphenylphosphoryl)-9-(4-(diphenylphosphoryl)phenyl)-9*H*-carbazole) was introduced as the host material (HOMO = −6.21 eV),

which has a similar transport capability of holes and electrons ($\mu_h = 9 \times 10^{-6} \text{ cm}^2 \text{ V}^{-1} \text{ s}^{-1}$ and $\mu_e = 3.0 \times 10^{-6} \text{ cm}^2 \text{ V}^{-1} \text{ s}^{-1}$).⁴ mCP (*N,N'*-dicarbazolyl-3,5-benzene) was added as another hole transport layer to lower the HOMO energy barrier between TAPC and PPO21,¹⁰ which was also used as the host material in the double EML devices. The molecular structures of materials above are also shown in Fig. 1.

In our previous report, graded distribution of the HOMO levels of TAPC (−5.50 eV), mCP (−5.90 eV), PPO21 (−6.21 eV) and the LUMO levels of TmPyPB (−2.70 eV), PPO21 (−2.68 eV), mCP (−2.30 eV) is beneficial for the injection and transport of holes and electrons, respectively.¹¹ Thus, balanced distribution of carriers and wide recombination zone could be expected in our device structure. Furthermore, the HOMO and LUMO levels of **Ir(BTBP)₂POP** (−5.58 eV and −2.76 eV, respectively) are within those of PPO21, carrier trapping is conceived to be the dominant EL mechanism of these devices.¹²

To optimize the doping concentration of **Ir(BTBP)₂POP**, three single EML devices with the structure of ITO/ MoO_3 (5 nm)/TAPC (30 nm)/mCP (5 nm)/PPO21:**Ir(BTBP)₂POP** (*x* wt%, 10 nm)/TmPyPB (20 nm)/LiF (1 nm)/Al (100 nm) were fabricated and studied by adjusting *x* to be 6 (DS1), 8 (DS2), 10 (DS3), respectively. Fig. 2 lists the EL spectra at 8 V, the doping concentration dependence of current density–luminance–voltage, current efficiency–luminance and power efficiency–luminance characteristics of these devices. The EL performances of these devices were summarized in Table 1. From Fig. 2(a) it can be observed that the similarity of the EL and PL (ESI, Fig. S2†) spectra indicates that the EL is caused by emission from the triplet excited states of the iridium complex **Ir(BTBP)₂POP**. The absence of residual emission from PPO21 suggests a complete energy transfer from the host to the dopant in these devices under the electric excitation.

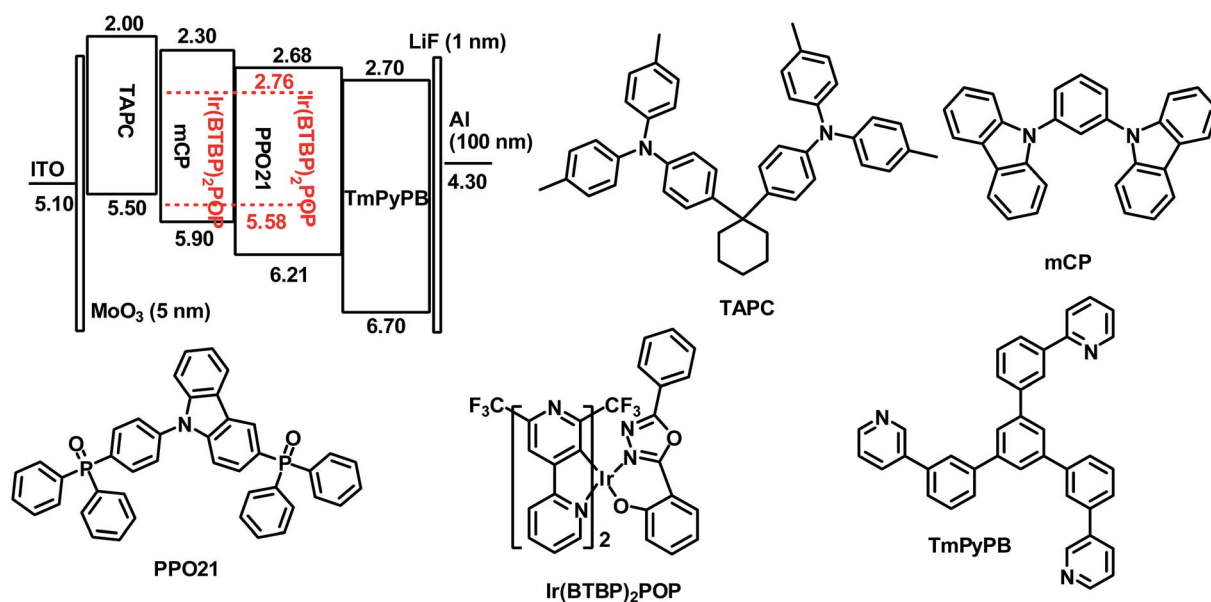


Fig. 1 Energy level diagram of HOMO and LUMO levels (relative to vacuum level) for materials investigated in this study and their molecular structures.



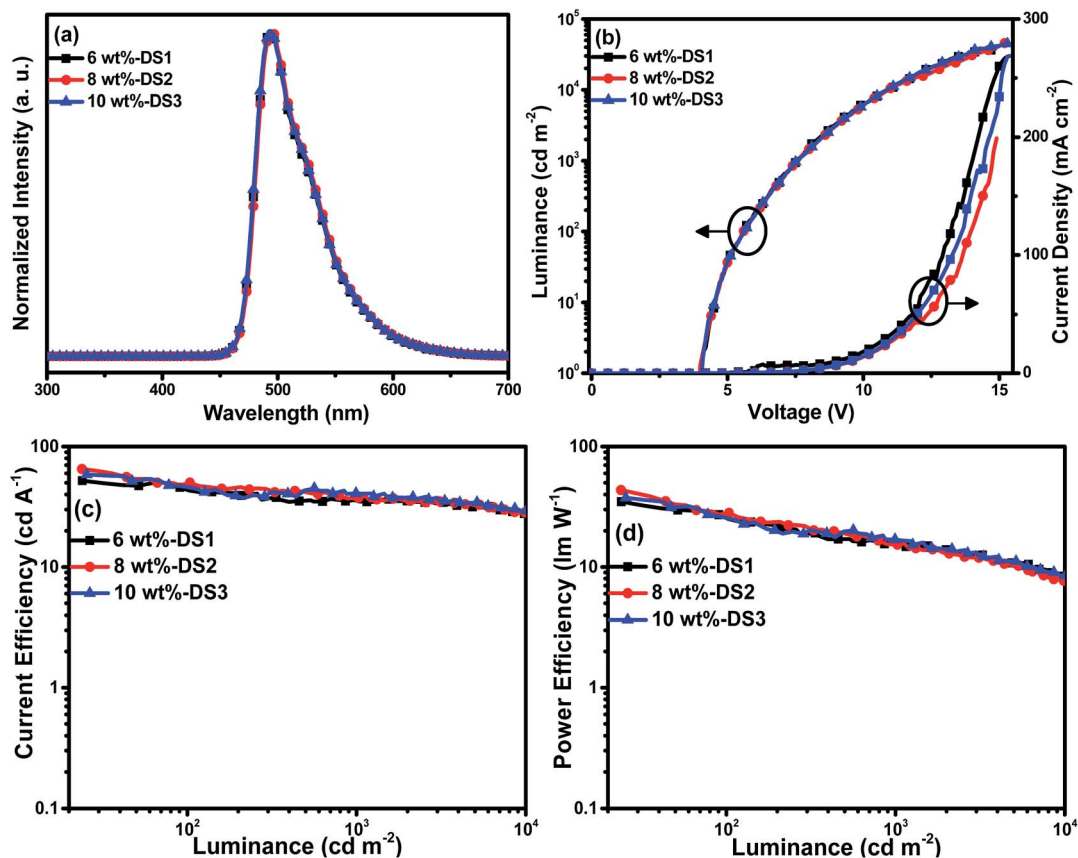


Fig. 2 Characteristics of single EML devices with Ir(BTBP)₂POP at different doping concentrations: (a) normalized EL spectra at 8 V; (b) current density–luminance–voltage (J – L – V) curves; (c) current efficiency–luminance (η_c – L) curves and (d) power efficiency–luminance (η_p – L) curves.

Table 1 EL performances of single EML devices with different doping concentrations of Ir(BTBP)₂POP

Device	Dopant concentration	$V_{\text{turn-on}}^a$ (V)	L_{max}^b [cd m^{-2} (V)]	$\eta_{c,\text{max}}^c$ (cd A^{-1}) ($\text{EQE}_{\text{max}}^d$)	$\eta_{c,L1000}^e$ (cd A^{-1}) (EQE_{L1000}^f)	$\eta_{p,\text{max}}^g$ (lm W^{-1})	λ_{max}^h (nm)	CIE ⁱ (x, y)
DS1	6 wt%	4.1	36 549 (14.7)	52.1 (18.7%)	34.9 (12.5%)	34.8	493	0.19, 0.54
DS2	8 wt%	4.0	45 445 (15.2)	65.1 (23.4%)	37.6 (13.5%)	43.5	494	0.19, 0.55
DS3	10 wt%	4.1	44 872 (15.3)	58.7 (21.1%)	40.7 (14.6%)	37.6	493	0.19, 0.54

^a Turn-on voltage recorded at a luminance of 1 cd m^{-2} . ^b Maximum luminance. ^c Maximum current efficiency. ^d Maximum external quantum efficiency. ^e Current efficiency at 1000 cd m^{-2} . ^f EQE at 1000 cd m^{-2} . ^g Maximum power efficiency. ^h Values were collected at 8 V. ⁱ Commission Internationale de l'Eclairage coordinates (CIE) at 8 V.

Results suggested that 8 wt% is the optimal concentration of Ir(BTBP)₂POP for the single EML devices. As shown in Table 1, the 8 wt% doped device (DS2) achieved the highest luminance, current efficiency, power efficiency and external quantum efficiency (EQE) of 45 445 cd m^{-2} , 65.1 cd A^{-1} , 43.5 lm W^{-1} and 23.4%, respectively. It can also be observed that the turn on voltages of these devices are high (around 4.0 V) though the dopants have good electron mobility, and the charge transport ability of TAPC/TmPyPB is also excellent. One reason is that the carrier mobility of the host material PPO21 is low ($\mu_h = 9 \times 10^{-6} \text{ cm}^2 \text{ V}^{-1} \text{ s}^{-1}$ and $\mu_e = 3.0 \times 10^{-6} \text{ cm}^2 \text{ V}^{-1} \text{ s}^{-1}$).⁴ Furthermore, the insertion of mCP would also cause energy loss during the current flow. These two factors may lead to the high turn-on

voltages of the devices. Moreover, the efficiency roll-off is somehow apparent, the current efficiency and EQE decreased to 37.6 cd A^{-1} and 13.5% as the luminance increased to 1000 cd m^{-2} , because of the poor carrier mobility of PPO21.

To further improve the EL performances of Ir(BTBP)₂POP, more devices were fabricated by optimizing the thickness of EML and ETL based on the 8 wt% doped single EML device. The EL performances of devices with different thickness of EML or ETL were shown in Fig. 3 and Table 2. From the curves and values in Table 2 it can be observed that the device luminance and efficiency increase firstly to a maximum value and then decrease gradually with increasing thickness of ETL by keeping the thickness of EML constant as 10 nm. The device DS5 with



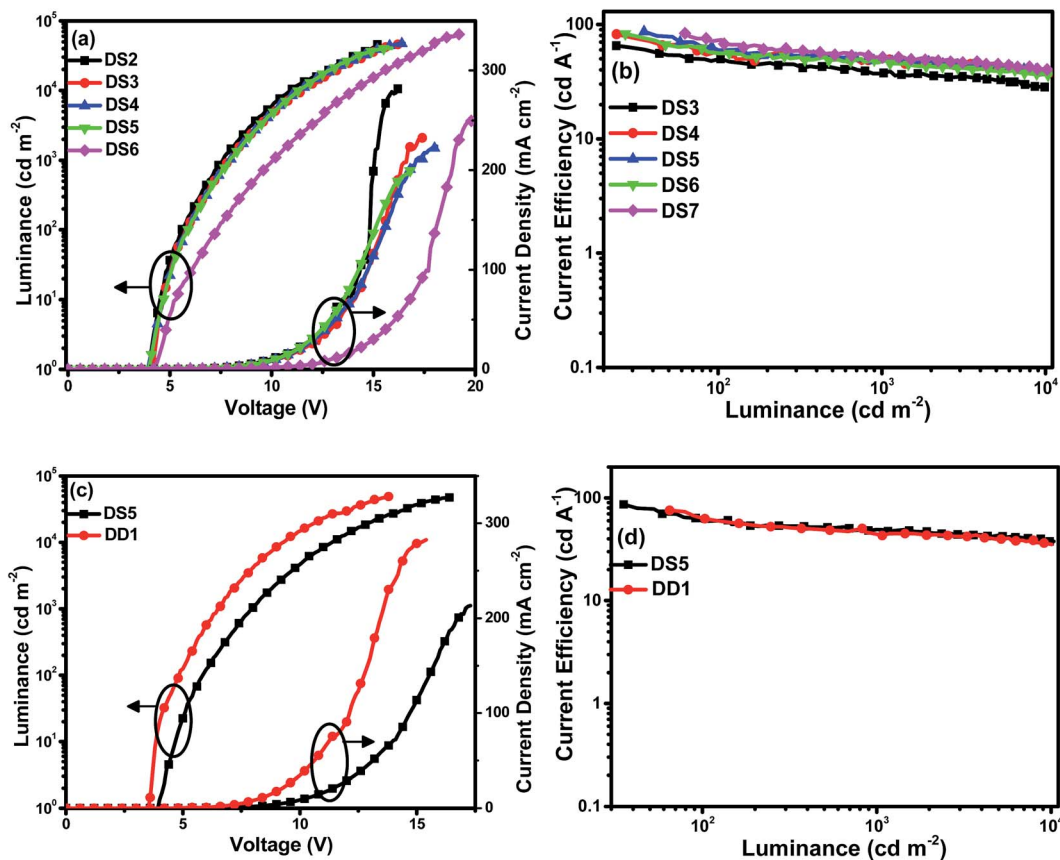


Fig. 3 (a) Current density–luminance–voltage (J – L – V), (b) current efficiency–luminance (η_c – L) curves of single EML devices (DS2, DS4–DS7) with different thickness of EML or ETL and (c) current density–luminance–voltage (J – L – V), (d) current efficiency–luminance (η_c – L) curves of single EML device DS5 and double EML device DD1.

Table 2 EL performances of devices with different thickness of EML or ETL

Device	EML ^a (nm)	ETL ^b (nm)	$V_{\text{turn-on}}^c$ (V)	L_{max}^d [cd m^{-2} (V)]	$\eta_{c,\text{max}}^e$ (cd A^{-1}) (EQE _{max} ^f)	$\eta_{c,L1000}^g$ (cd A^{-1}) (EQE _{L1000} ^h)	$\eta_{p,\text{max}}^i$ (lm W^{-1})
DS2	10	20	4.0	45 445 (15.2)	65.1 (23.4%)	37.6 (13.5%)	43.5
DS4	10	30	4.2	46 743 (16.4)	82.0 (29.4%)	49.5 (17.8%)	51.5
DS5	10	40	4.0	47 599 (16.5)	86.5 (31.0%)	49.2 (17.6%)	52.2
DS6	10	50	4.0	40 624 (15.9)	82.8 (29.7%)	48.4 (17.4%)	51.0
DS7	15	40	4.3	63 954 (19.2)	83.7 (30.0%)	51.5 (18.5%)	37.5
DD1	—	—	3.6	49 139 (13.9)	75.8 (27.2%)	43.0 (15.4%)	51.7

^a Thickness of EML. ^b Thickness of ETL. ^c Turn-on voltage recorded at a luminance of 1 cd m^{-2} . ^d Maximum luminance. ^e Maximum current efficiency. ^f Maximum external quantum efficiency. ^g Current efficiency at 1000 cd m^{-2} . ^h EQE at 1000 cd m^{-2} . ⁱ Maximum power efficiency.

40 nm ETL achieved the best device performances with maximum luminance, current efficiency, power efficiency and EQE of $47 599 \text{ cd m}^{-2}$, 86.5 cd A^{-1} , 52.2 lm W^{-1} and 31.0%, respectively. With increasing thickness of ETL, the increasing electron transport balanced injection and recombination of charge carriers and decreased electron density within EML. As a result, the distribution of holes and electrons tended to balance firstly and then deteriorated gradually when the thickness of ETL was thicker than 40 nm.

Furthermore, the device DS7 with 15 nm EML was also fabricated based on the device DS5. It can be seen that DS7 has

higher luminance ($63 954 \text{ cd m}^{-2}$) and little lower efficiencies (83.7 cd A^{-1} , 37.5 lm W^{-1} and EQE 30.0%) than that of DS5. The increased thickness of EML caused larger recombination zone and fewer recombination probabilities, within which more dopants were excited to emit but fewer charge carriers recombined, in result of higher luminance and lower efficiencies.

Subsequently, the double EMLs device DD1 with the structure of ITO/MoO₃ (5 nm)/TAPC (30 nm)/mCP:Ir(BTBP)₂POP (8 wt%, 10 nm)/PPO21:Ir(BTBP)₂POP (8 wt%, 10 nm)/TmPyPB (40 nm)/LiF (1 nm)/Al (100 nm) was also fabricated. The EL characteristics of single EML device DS5 and double EML device



DD1 are shown in Fig. 3 and Table 2. In most cases, the double EMLs devices will broaden the exciton formation zone, in result of high efficiency and low efficiency roll-off. But compared with DS5, double EML device DD1 obtained a higher maximum luminance of 49 139 cd m^{-2} and lower maximum current efficiency, power efficiency and EQE of 75.8 cd A^{-1} , 51.7 lm W^{-1} and 27.2%, respectively, and the efficiencies declined obviously as the luminance increased, while the turn-on voltage of 3.6 V was much lower than DS5. The usage of double EML led to the lower charge injection barrier and broadening recombination zone, resulting in the lower turn-on voltage and higher luminance than the single EML device. However, the reduced efficiencies and the high efficiency roll-off were probably due to the poor electron mobility of mCP and PPO21, especially under the high electric field, which would cause the imbalanced injection, transport and recombination of carriers, leading to the lower efficiencies and the high efficiency roll-off.

Experimental section

OLEDs fabrication and measurement

The **Ir(BTBP)₂POP** complex was prepared in our laboratory (ESI[†]) with emission peak at 503 nm, photoluminescence quantum yield (Φ_p) of 88%, phosphorescence lifetime (τ) of 2.86 μs in degassed CH_2Cl_2 solution and HOMO/LUMO levels of $-5.58/-2.76$ eV in deaerated solution ($\text{CH}_2\text{Cl}_2 : \text{CH}_3\text{CN} = 1 : 1$). All OLEDs with the emission area of 0.1 cm^2 were fabricated on the pre-patterned ITO-coated glass substrate with a sheet resistance of 15 $\Omega \text{ sq}^{-1}$. All chemicals used for devices were sublimed in vacuum (2.0×10^{-4} Pa) prior to use. The deposition rate for organic compounds is 1–2 \AA s^{-1} . The phosphor and host were co-evaporated from two separate sources. The cathode consisting of LiF/Al was deposited by evaporation of LiF with a deposition rate of 0.1 \AA s^{-1} and then by evaporation of Al metal with a rate of 3 \AA s^{-1} . The effective area of the emitting diode is 0.1 cm^2 . The characteristics of the devices were measured with a computer controlled KEITHLEY 2400 source meter with a calibrated silicon diode in air without device encapsulation. On the basis of the uncorrected PL and EL spectra, the CIE coordinates were calculated using a test program of the Spectra scan PR650 spectrophotometer.

Conclusions

In this work, we synthesized a novel heteroleptic Ir(III) complex (**Ir(BTBP)₂POP**) using 2',6'-bis(trifluoromethyl)-2,4'-bipyridine (BTBP) as the main ligand and 2-(5-phenyl-1,3,4-oxadiazol-2-yl) phenol (HPOP) as the ancillary ligand. A series of devices using **Ir(BTBP)₂POP** as the emitter with single or double EML(s) were fabricated and compared. To balance the distribution of holes and electrons, not only the doping concentration but also the thicknesses of EML and ETL were experimentally optimized. Finally, efficient green device with maximum luminance, current efficiency, power efficiency and EQE up to 47 599 cd m^{-2} , 86.5 cd A^{-1} , 52.2 lm W^{-1} and 31.0%, respectively, was realized. The high efficiency of the device suggests the complex has potential applications in OLEDs.

Acknowledgements

This work was supported by the National Natural Science Foundation of China (21371093, 91433113), the Major State Basic Research Development Program (2013CB922101) and the Natural Science Foundation of Jiangsu Province (BK20130054).

Notes and references

- (a) C. W. Tang, S. A. VanSlyke and C. H. Chen, *J. Appl. Phys.*, 1989, **65**, 3610; (b) M. A. Baldo, D. F. O'Brien, Y. You, A. Shoustikov, S. Sibley, M. E. Thompson and S. R. Forrest, *Nature*, 1998, **395**, 151; (c) H. Sun, S. Liu, W. Lin, K. Y. Zhang, W. Lv, X. Huang, F. Huo, H. Yang, G. Jenkins, Q. Zhao and W. Huang, *Nat. Commun.*, 2014, **5**, 3601; (d) P. Tao, W. L. Li, J. Zhang, S. Guo, Q. Zhao, H. Wang, B. Wei, S. J. Liu, X. H. Zhou, Q. Yu, B. S. Xu and W. Huang, *Adv. Funct. Mater.*, 2016, **26**, 881; (e) K. Y. Zhang, X. Chen, G. Sun, T. Zhang, S. Liu, Q. Zhao and W. Huang, *Adv. Mater.*, 2016, **28**, 7137.
- (a) X. K. Liu, W. C. Chen, H. T. Chandran, J. Qing, Z. Chen, X. H. Zhang and C. S. Lee, *ACS Appl. Mater. Interfaces*, 2016, **8**, 26135; (b) H. A. Al Attar and A. P. Monkman, *Adv. Mater.*, 2016, **28**, 8014; (c) H. W. Mo, Y. Tsuchiya, Y. Geng, T. Sagawa, C. Kikuchi, H. Nakanotani, F. Ito and C. Adachi, *Adv. Funct. Mater.*, 2016, **26**, 6703; (d) R. Gómez-Bombarelli, J. Aguilera-Iparraguirre, T. D. Hirzel, D. Duvenaud, D. Maclaurin, M. A. Blood-Forsythe, H. S. Chae, M. Einzinger, D. G. Ha, T. Wu, G. Markopoulos, S. Jeon, H. Kang, H. Miyazaki, M. Numata, S. Kim, W. Huang, S. I. Hong, M. Baldo, R. P. Adams and A. Aspuru-Guzik, *Nat. Mater.*, 2016, **15**, 1120; (e) Y. H. Zhou, Q. L. Xu, H. B. Han, Y. Zhao, Y. X. Zheng, L. Zhou, J. L. Zuo and H. J. Zhang, *Adv. Opt. Mater.*, 2016, **4**, 1726.
- (a) S. Lamansky, P. Djurovich, D. Murphy, F. Abdel-Razzaq, H. E. Lee, C. Adachi, P. E. Burrows, S. R. Forrest and M. E. Thompson, *J. Am. Chem. Soc.*, 2001, **123**, 4304; (b) F. Han, X. Zhang, J. Zhang, Y. Wei, X. Zhang, W. Huang and H. Xu, *Chem. Commun.*, 2016, **52**, 5183; (c) J. X. Cai, T. L. Ye, X. F. Fan, C. M. Han, H. Xu, L. L. Wang, D. G. Ma, Y. Lin and P. F. Yan, *J. Mater. Chem.*, 2011, **21**, 15405; (d) H. Xu, R. Chen, Q. Sun, W. Lai, Q. Su, W. Huang and X. Liu, *Chem. Soc. Rev.*, 2014, **43**, 3259; (e) F. Q. Han, C. M. Han and H. Xu, *Chin. Chem. Lett.*, 2016, **27**, 1193.
- W. S. Jeon, T. J. Park, S. Y. Kim, R. Pode, J. Jang and J. H. Kwon, *Appl. Phys. Lett.*, 2008, **93**, 063303.
- Q. L. Xu, X. Liang, S. Zhang, Y. M. Jing, X. Liu, G. Z. Lu, Y. X. Zheng and J. L. Zuo, *J. Mater. Chem. C*, 2015, **3**, 3694.
- Y. Tao, C. Yang and J. Qin, *Chem. Soc. Rev.*, 2011, **40**, 2943.
- (a) H. Y. Li, T. Y. Li, M. Y. Teng, Q. L. Xu, S. Zhang, Y. M. Jin, X. Liu, Y. X. Zheng and J. L. Zuo, *J. Mater. Chem. C*, 2014, **2**, 1116; (b) Y. M. Jing, C. C. Wang, L. S. Xue, T. Y. Li, S. Zhang, X. Liu, X. Liang, Y. X. Zheng and J. L. Zuo, *J. Organomet. Chem.*, 2014, **765**, 39.
- J. Lee, N. Chopra, S. H. Eom, Y. Zheng, J. Xue, F. So and J. Shi, *Appl. Phys. Lett.*, 2008, **93**, 123306.



- 9 S. J. Su, T. Chiba, T. Takeda and J. Kido, *Adv. Mater.*, 2008, **20**, 2125.
- 10 P. Borsenberger, L. Pautmeier, R. Richert and H. Bässler, *J. Chem. Phys.*, 1991, **94**, 8276.
- 11 (a) Q. L. Xu, X. Liang, S. Zhang, Y. M. Jing, X. Liu, G. Z. Lu, Y. X. Zheng and J. L. Zuo, *J. Mater. Chem. C*, 2015, **3**, 3694; (b) Q. L. Xu, X. Liang, L. Jiang, Y. Zhao and Y. X. Zheng, *RSC Adv.*, 2015, **5**, 89218; (c) Q. L. Xu, X. Liang, L. Jiang, Y. Zhao and Y. X. Zheng, *Dalton Trans.*, 2016, **45**, 7366.
- 12 (a) M. Ikai, S. Tokito, Y. Sakamoto, T. Suzuki and Y. Taga, *Appl. Phys. Lett.*, 2001, **79**, 156; (b) M. Uchida, C. Adachi, T. Koyama and Y. Taniguchi, *J. Appl. Phys.*, 1999, **86**, 1680.

